Moving Finite Elements and Dynamic Vehicle Interaction

Hakan Lane, Per Kettil, Nils-Erik Wiberg

Moving Finite Elements and Dynamic Vehicle Interaction

Hakan Lane, Per Kettil, Nils-Erik Wiberg

PII: S0997-7538(07)00094-0
DOI: 10.1016/j.euromechsol.2007.09.007
Reference: EJMSOL 2382

To appear in: *European Journal of Mechanics A/Solids*

Received date: 24 July 2006
Accepted date: 25 September 2007

Please cite this article as: H. Lane, P. Kettil, N.-E. Wiberg, Moving Finite Elements and Dynamic Vehicle Interaction, *European Journal of Mechanics A/Solids* (2007), doi: 10.1016/j.euromechsol.2007.09.007

MOVING FINITE ELEMENTS

AND

DYNAMIC VEHICLE INTERACTION

Hakan Lane[*], Per Kettil[*] and Nils-Erik Wiberg[*]

[*] Department of Applied Mechanics
Chalmers University of Technology
Gothenburg, Sweden
E-mail: Hakan.Lane@sm.chalmers.se

Key words: Moving Finite Elements, Rigid Body Dynamics, Rail Induced Vibrations

Abstract: *Elastic "shock" waves emanating from the wheel-rail interface of a train running at a speed close to one of the propagation velocities of the soil may cause great amounts of nuisances to the population. An integrated rigid body – FEM model has been created in order to advance the understanding of these effects and predict the effects of different countermeasures. Usage of a fixed mesh includes more elements than necessary for an accurate solution and limits the analysis to a rather short distance.*

This paper replaces a large fixed mesh with a smaller mobile grid. A special algorithm has been developed to ensure that the nodes are translated with the same speed as the passing vehicle. The values of fields are updated through an interpolation procedure.

Results indicate that a size of about 15 m in front of and behind the wheel-rail interfaces is enough to ensure the same results as the fixed mesh in a fraction of the time. The initial transient phase is followed by a relatively constant wave pattern being transported underneath the train. Waves are shown to be greatly magnified if the speed of the system exceeds the Rayleigh velocity of the top layer of crust.

1 INTRODUCTION

A properly designed railway infrastructure is a vital part of a sustainable transport system for the future. Intense competition for higher shares of the transportation market has lead to a drive towards more high speed trains on the European rail network. As a consequence, the speed of the train may now surpass one of the wave propagation velocities in the soil. When this occurs, elastic solid waves can be emitted from the sleepers and propagate to surrounding buildings. Resonance may lead to rather disturbing effects for people inside and in some causes even harm the operation of delicate electronic equipment. Rail maintenance companies are faced with the task of mitigating these vibrations. Computational modeling is a vital part of this task.

An integrated rail vehicle – track structure model has been created for the purpose of predicting and analyzing solid elastic waves in rail systems (Lane et al., 2005). However, the

required time and computational resources restricts the size of the model quite severely. In some various studies presented so far (Larsson and Berg, 2005), (Ching 2004), only 89 metres of rail have been analysed. Simulations of the behaviour over longer stretches require that the finite element grid is moved together with the excitation provided by the weight of the rigid body.

Much work has been performed on the application of a "moving mesh" or "moving grid" approach to the solution of PDE:s (Baines 2002). Also known as *r* adaptivity, it has been used to simulate vastly different physical systems (Forster et al., 2002), (Gwynllyw et al., 1996), (Budd and Collins, 1998). The basic idea is to move the nodes and elements in the discretisation based on some kind of algorithm, criterion or measure.

As the coupling between the wheels and the rail occur through specially labeled constraint equations, the speed of the rigid body can be measured from the elastic domain by the movement of the algebraic mean of the position of the wheel contact points. As the target is to keep the body in the mid region of the finite element domain in a plane normal to the direction of travel, the mesh should be displaced with the rate of motion of the wheels as indicated by their mean position. This article presents an algorithm to achieve this kind of mesh adaptivity incorporating the option to introduce new directions (e.g. slopes, transitions, curves) at the front of the grid while also correctly interpolating node field variables (displacements, velocities, accelerations) and element fields (stress, external and internal strains and energy) from the old positions to the new ones.

The outline is as follows: Chapter 2 presents the computational model and how local system matrices are established, Chapter 3 how time integration of the assembled system is performed with a Newmark algorithm, Chapter 4 how the motion of the nodes are coupled to the speed of the impeding vehicle, Chapter 5 discusses how the state is interpolated from one position to the next, Chapter 6 presents the results of simulations with a model of an X2 locomotive running at different velocities and Chapter 7 gives some conclusions of the study.

2 INTEGRATED RIGID BODY FEM MODEL

2.1 Overview

The computational building blocks are (see Figure 1):

- A train described by rigid body dynamics including dynamic motion laws for the reference point, a Bryant angular representation (Wittenburg 1977) and constraints.
- The rigid bodies are connected through 3D stiffness / damping connectors.
- A 3D linear finite element model of the track structure and parts of the subgrade including rail, sleepers, ballast, dry crust and layers of clay. The entire model is built on solid eight node brick elements (MacNeal 1994). There are also some multi point constraints between the displacements of nodes of different layers for matching purposes. These have been inserted at the interfaces of the submeshes between rail and sleepers and sleepers and ballast. The complex geometry at the top of the track foundation leads to the requirement to bring together several separate grids.

- Constraint equations keeping the virtual nodes for the wheel contact on the rail surface. They are generated in each time step through an especially developed dynamic differential generation algorithm, whereby the location of the point is used to tie the change in displacements for the wheel to the change in displacements of the nodes on the top of the rail in the element that the wheel will be moved to (Lane et. al., 2004). The gravity load applied to the rigid body reference point is transferred to the ground numerically through the associated Lagrange multipliers.
- The mesh with elastic materials is supplemented by viscoelastic boundary layers. The dimensions and material properties are chosen to create non-reflecting boundaries at interfaces to "infinite" regions of soil around the subgrade. The details are provided by Lane et. al. (Lane et al., 2006). The degrees of freedom at the outer ends of the boundary layers are fixed in all directions.

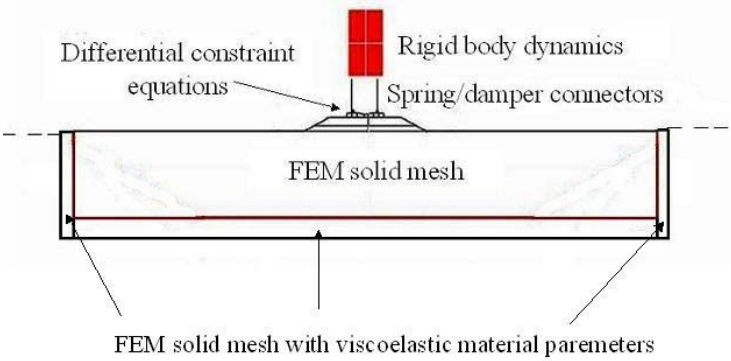

Figure 1: Compound analysis model.

The approach to solve the problem with equations from several sources was presented by Lane *et. al.* (Lane et. al., 2004). The equations for the rigid body and connectors are integrated with the finite element terms into a single, global system. The unknowns are the degrees of freedom in the soil, the body centers of gravity, the generalized degrees of freedom on either side of each connector and Lagrange multipliers for the restraints as modeled by constraint equations and boundary conditions.

2.2 Governing equations and assembly process

Each part of the system (finite element, body, connector, constraint, boundary condition) is referred to as an element. Based on a local set of degrees of freedom $\mathbf{u}_e$, the equations for the various realms leads to dynamic local matrices for mass ($\mathbf{M}_e$), stiffness ($\mathbf{K}_e$), damping ($\mathbf{C}_e$) and an internal force $\mathbf{F}_{int}$. The generation of these terms are based on the dynamic equations and carried out as follows.

2.2.1 Elastic soil motion

In the absence of externally applied forces, elastic wave propagation in a soil with with density ρ and viscosity υ is ruled by the following relationship between displacements **u**,

stresses $\boldsymbol{\sigma}$:

$$-\tilde{\nabla}^T\boldsymbol{\sigma} + \upsilon\,\dot{\mathbf{u}} + \rho\,\ddot{\mathbf{u}} = \mathbf{0} \tag{1}$$

The gradient operator $\tilde{\nabla}$ is defined as (Samuelsson and Wiberg, 1998)

$$\tilde{\nabla} = \begin{bmatrix} \frac{\partial}{\partial x} & 0 & 0 \\ 0 & \frac{\partial}{\partial y} & 0 \\ 0 & 0 & \frac{\partial}{\partial z} \\ \frac{\partial}{\partial y} & \frac{\partial}{\partial x} & 0 \\ 0 & \frac{\partial}{\partial z} & \frac{\partial}{\partial y} \\ \frac{\partial}{\partial z} & 0 & \frac{\partial}{\partial x} \end{bmatrix} \tag{2}$$

Based on the Young's modulus *E,* the viscosity υ and the poisson ratio *v*, the constitutive relationship between stresses and strains

$$\boldsymbol{\sigma} = \mathbf{D}\boldsymbol{\varepsilon} + \mathbf{C}_\upsilon\dot{\boldsymbol{\varepsilon}} = \mathbf{D}\tilde{\nabla}\,\mathbf{u} + \mathbf{C}_\upsilon\tilde{\nabla}\,\dot{\mathbf{u}} \tag{3}$$

is dependent on both the strain and the strain rate. A Kelvin material model (parallel stiffness and damping operators) is used. It applies the constitutive matrices

$$\mathbf{D} = \frac{E}{2(1+\nu)}\begin{bmatrix} \frac{2(1-\nu)}{1-2\nu} & \frac{2\nu}{1-2\nu} & \frac{2\nu}{1-2\nu} & 0 & 0 & 0 \\ \frac{2\nu}{1-2\nu} & \frac{2(1-\nu)}{1-2\nu} & \frac{2\nu}{1-2\nu} & 0 & 0 & 0 \\ \frac{2\nu}{1-2\nu} & \frac{2\nu}{1-2\nu} & \frac{2(1-\nu)}{1-2\nu} & 0 & 0 & 0 \\ 0 & 0 & 0 & 1 & 0 & 0 \\ 0 & 0 & 0 & 0 & 1 & 0 \\ 0 & 0 & 0 & 0 & 0 & 1 \end{bmatrix} \tag{4}$$

and

$$\mathbf{C}_v = \frac{v}{2(1+\nu)} \begin{bmatrix} \frac{2(1-\nu)}{1-2\nu} & \frac{2\nu}{1-2\nu} & \frac{2\nu}{1-2\nu} & 0 & 0 & 0 \\ \frac{2\nu}{1-2\nu} & \frac{2(1-\nu)}{1-2\nu} & \frac{2\nu}{1-2\nu} & 0 & 0 & 0 \\ \frac{2\nu}{1-2\nu} & \frac{2\nu}{1-2\nu} & \frac{2(1-\nu)}{1-2\nu} & 0 & 0 & 0 \\ 0 & 0 & 0 & 1 & 0 & 0 \\ 0 & 0 & 0 & 0 & 1 & 0 \\ 0 & 0 & 0 & 0 & 0 & 1 \end{bmatrix} \tag{5}$$

The matrices for a soil element with the nodal displacements $\mathbf{u}_i$, i = 1,2,...,8, the material density ρ density of the material and the constitutive stress-strain matrix **D** (eq. 4) are generated from standard finite element procedures based on the shape functions **N** and their spatial derivatives $\mathbf{B} = \tilde{\nabla}\,\mathbf{N}$ **:**

$$\mathbf{u_e} = [\mathbf{u}_1\ \mathbf{u}_2\ \mathbf{u}_3\ \mathbf{u}_4\ \mathbf{u}_5\ \mathbf{u}_6\ \mathbf{u}_7\ \mathbf{u}_8]^{\mathrm{T}} \tag{6}$$

$$\mathbf{M_e} = \int \mathbf{N}^{\mathrm{T}} \rho \mathbf{N} dV \tag{7}$$

$$\mathbf{K_e} = \int \mathbf{B}^{\mathrm{T}} \mathbf{D} \mathbf{B} dV \tag{8}$$

$$\mathbf{C_e} = 0.001\mathbf{K_e} + 0.001\mathbf{M_e} \tag{9}$$

$$\mathbf{F_{int}} = \int \mathbf{B}^{\mathrm{T}} \mathbf{D} \mathbf{B} \mathbf{u} dV + \mathbf{M_e}\ddot{\mathbf{u}}_\mathbf{e} + \mathbf{C_e}\dot{\mathbf{u}}_\mathbf{e} \tag{10}$$

The Rayleigh approach was applied for the elastic domain. For a material with a visco-elastic material model, the damping term $\mathbf{C_e}$ is derived as

$$\mathbf{C_e} = \int \mathbf{B}^{\mathrm{T}} \mathbf{C}_v \mathbf{B} dV \tag{11}$$

This is used in the absorbing layers.

2.2.2 Rigid bodies and connecting elements

The definition of a set of elements making up a rigid body is that it is undeformable, i.e. the distance between any set of two points remains constant through time. The inertial properties are the mass m and the rotary inertia tensor **J** and the body is subject to a gravitational acceleration $\mathbf{a} = [0\ 0\ -g]^{\mathrm{T}}$. A linear small angle approximation has been chosen. Based on the displacements $\mathbf{u_r}$ of a *reference point* (usually the center of gravity) and a set of Bryant angles $\boldsymbol{\varphi} = [\varphi_1\ \varphi_2\ \varphi_3]^{\mathrm{T}}$ describing the state of rotation, the Lagrange equations based on

minimizing the functional of the energy

$$E = T - P \tag{12}$$

based on the kinetic energy

$$T = \frac{1}{2} m\mathbf{I}(\dot{\mathbf{u}}_r{}^T \dot{\mathbf{u}}_r) + \frac{1}{2}\mathbf{J}(\dot{\boldsymbol{\varphi}}^T \dot{\boldsymbol{\varphi}}) \tag{13}$$

and the potential

$$P = \mathrm{m}\mathbf{a}^{\mathrm{T}}\mathbf{u}_{\mathbf{r}} \tag{14}$$

become

$$\frac{d}{dt}\left(\frac{\partial T}{\partial \dot{u}_i}\right) - \frac{\partial T}{\partial u_i} = -\frac{\partial P}{\partial u_i} \tag{15}$$

The vector

$$\mathbf{u} = [\mathbf{u}_\mathbf{r}\ \boldsymbol{\varphi}]^{\mathrm{T}} \tag{16}$$

includes translational and rotational degrees of freedom for the reference point.

The application of the dynamic Lagrange equations in the assembly process leads to the matrices

$$\mathbf{u}_\mathbf{e} = [\mathbf{u}_\mathbf{r}\ \boldsymbol{\varphi}]^{\mathrm{T}} \tag{17}$$

$$\mathbf{K}_\mathbf{e} = \mathbf{C}_\mathbf{e} = \mathbf{0}_3 \tag{18}$$

$$\mathbf{M}_\mathbf{e} = \begin{bmatrix} m\mathbf{I}_3 & \mathbf{0}_3 \\ \mathbf{0}_3 & \mathbf{J} \end{bmatrix} \tag{19}$$

$$\mathbf{F}_{\mathbf{int}} = \mathbf{M}_\mathbf{e}\ddot{\mathbf{u}}_\mathbf{e} \tag{20}$$

The notation $\mathbf{0}_3$ refers to the 3x3 zero matrix and $\mathbf{I}_3$ to the corresponding unit matrix. The internal force vector contains inertial terms both for the translational and rotary degrees of freedom.

As can be viewed in Figure 2, a connector is a spring/damper combination between two points. It has been used to represent the suspensions between the bodies making up the train and as a model of the contact between wheel and rail.

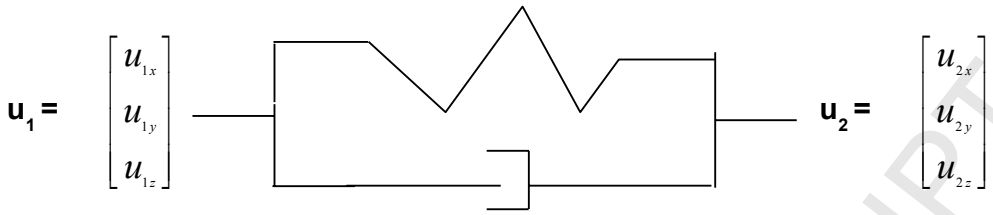

Figure 2: Connector.

The spring is defined by the 3x3 stiffness matrix

$$\mathbf{K} = \begin{bmatrix} K_{xx} & K_{xy} & K_{xz} \\ & K_{yy} & K_{yz} \\ symmetric & & K_{zz} \end{bmatrix} \tag{21}$$

and the damper by the corresponding entity

$$\mathbf{C} = \begin{bmatrix} C_{xx} & C_{xy} & C_{xz} \\ & C_{yy} & C_{yz} \\ symmetric & & C_{zz} \end{bmatrix} \tag{22}$$

As the relative distance $\mathbf{u_2} - \mathbf{u_1}$ or the corresponding relative velocity $\dot{\mathbf{u}}_2 - \dot{\mathbf{u}}_1$ is altered, the system reacts by the internal force

$$\mathbf{F_{int}} = \mathbf{K}(\mathbf{u_2} - \mathbf{u_1}) + \mathbf{C}(\dot{\mathbf{u}}_2 - \dot{\mathbf{u}}_1) \tag{23}$$

This yields the numerical terms

$$\mathbf{u_e} = [\mathbf{u}_1\ \mathbf{u}_2]^T \tag{24}$$

$$\mathbf{K_e} = \mathbf{K} \tag{25}$$

$$\mathbf{C_e} = \mathbf{C} \tag{26}$$

$$\mathbf{M_e} = \mathbf{0_3} \tag{27}$$

$$\mathbf{F_{int}} = \mathbf{K_e}\,(\mathbf{u_2} - \mathbf{u_1}) + \mathbf{C_e}\,(\dot{\mathbf{u}}_2 - \dot{\mathbf{u}}_1) \tag{28}$$

Here, $\mathbf{u_1}$ and $\mathbf{u_2}$ represent the displacements on either side of the joint, $\mathbf{K}$ the stiffness matrix (21) and $\mathbf{C}$ the corresponding damping values (22).

2.2.3 Constraint equations and boundary conditions

The equation for a holonomic constraint or boundary condition locking the displacements of one *slave* node $\mathbf{u_s}$ or connecting them to those of several master nodes $\mathbf{u_j}$ (j=1,2,…,N) is

$$\Phi = \sum_{i=1}^{ndof} C_{si} u_{si} + \sum_{j=1}^{N} \sum_{i=1}^{ndof} C_{ji} u_{ji} + A = 0 \tag{29}$$

Theory predicts that in the presence of a constraint $\mathbf{\Phi}$ ($\mathbf{u}$) = 0, there is a number λ such that the function F ($\mathbf{u}$) is minimised by the formula (Stahel 1999)

$$\nabla F(\mathbf{u}) + \lambda \nabla \Phi(\mathbf{u}) = \mathbf{0} \tag{30}$$

The vector λ contains the *Lagrange multipliers*. These numerical relationships are integrated to the common framework through the following definitions:

$$\mathbf{u_e} = [\mathbf{u_s}\ \mathbf{u_{j1}}\ \mathbf{u_{j2}}\ \ldots\ \mathbf{u_{jN}}\ \lambda_i]^{\mathrm{T}} \tag{31}$$

$$\mathbf{K_e} = \mathbf{C_e} = \mathbf{0} \tag{32}$$

$$\mathbf{M_e} = \begin{bmatrix} 0 & 0 & 0 & \cdots & \cdots & 0 & C_{s1} \\ 0 & \ddots & & & & & C_{s2} \\ 0 & & \ddots & & & & C_{s3} \\ \vdots & & & \ddots & & & C_{11} \\ \vdots & & & & \ddots & & \vdots \\ 0 & & & & & 0 & C_{N3} \\ C_{s1} & C_{s2} & C_{s3} & \cdots & \cdots & C_{N3} & 0 \end{bmatrix} \tag{33}$$

The internal force is based on the *value* of the constraint Φ (the deviation of (19) from the desired value of 0) according the formula

$$\begin{bmatrix} \lambda C_{s1} & \lambda C_{s1} & \lambda C_{s1} & \lambda C_{11} & \cdots & \lambda C_{N3} & \Phi \end{bmatrix} \tag{34}$$

Constraints are inserted to enforce rigid body conditions between the degrees of freedom of the center of gravity and connector points on a body, at interfaces between adjacent finite element meshes and between the virtual wheel point and the nodes on the rail surface.

3 NEWMARK TIME INTEGRATION

3.1 System of equations

Analysis is based on finding a state ($\mathbf{u}, \dot{\mathbf{u}}$, $\ddot{\mathbf{u}}$) matching the externally applied forces $\mathbf{F}_{ext}$ with the internal forces $\mathbf{F}_{int}$ ($\mathbf{u}, \dot{\mathbf{u}}$, $\ddot{\mathbf{u}}$) while also fulfilling the constraints $\mathbf{\Phi}$ ($\mathbf{u}$) = $\mathbf{0}$. The condition of minimum virtual work in the presence of a number of holonomic constraints leads to the formulation

$$\text{Find min} \int (\mathbf{F}_{ext} - \mathbf{F}_{int}(\mathbf{u}, \dot{\mathbf{u}}, \ddot{\mathbf{u}})) \, \delta u dV \tag{35}$$

$$\text{subject to } \mathbf{\Phi} = \mathbf{0} \tag{36}$$

Based on the theory of minimising a functional with a set of constraints as stated in (15), the target is to find a solution to the system of equations

$$\mathbf{F}_{ext} - \mathbf{F}_{int}(\mathbf{u}, \dot{\mathbf{u}}, \ddot{\mathbf{u}}) + \lambda \nabla \mathbf{\Phi} = \mathbf{0} \tag{37}$$

The terms in equation (36) are *global* vectors constructed through assembling the local contributions. Whereas the $\mathbf{F}_{ext}$ vector is made up of additions at degrees of freedom where external forces are applied (gravitational forces at the rigid bodies), the internal force vector $\mathbf{F}_{int}$ is made up from the elements as defined in Chapter 2.1 – 2.2. The term for the Lagrangian multipliers is described in Chapter 2.3 .

3.2 Scaling the terms

The numerical constants from the various parts show a great variation in their magnitude, leading to a badly conditioned system. In order to mitigate this problem, the constraint equations are scaled by multiplying all terms by a common value. This value is chosen by finding the smallest equation index among the participating nodes i_{min}.

3.3 Time Integration algorithm

The system of equations presented in (40) is solved by a Newmark predictor-corrector time integration scheme. Initial values of the statefields $\mathbf{u}, \dot{\mathbf{u}}$ and $\ddot{\mathbf{u}}$ are either set explicitly to 0, found from previous values or assigned by the user. For each subpart, the *local* element matrices for mass ($\mathbf{M}_e$), damping ($\mathbf{C}_e$) and stiffness ($\mathbf{K}_e$) are found from the assembly process discussed in Chapter 2. Before being inserted into the global system, they are merged into a dynamic mass matrix through the operation

$$\mathbf{M}_{*e} = \mathbf{M}_e + \alpha \Delta t \mathbf{C}_e + \beta \frac{(\Delta t)^2}{2} \mathbf{K}_e \tag{38}$$

The parameters α and β are the chosen Newmark parameters and Δt the time increment. The increments to the primary unknowns $\ddot{\mathbf{u}}$ and the Lagrange multipliers are similarly joined into the vector

$$\mathbf{a} = \begin{bmatrix} \ddot{\mathbf{u}} \\ \boldsymbol{\lambda} \end{bmatrix} \tag{39}$$

and the incremental entity

$$\boldsymbol{\delta a} = \begin{bmatrix} \boldsymbol{\delta}\ddot{\mathbf{u}} \\ \boldsymbol{\delta\lambda} \end{bmatrix} \tag{40}$$

For all subsequent time steps, the Newmark solution strategy is then initiated by a first prediction step

$$\dot{\mathbf{u}}_{n+1} = \dot{\mathbf{u}}_n + (1-\alpha)\,\Delta t\,\ddot{\mathbf{u}}_n \tag{41}$$

$$\mathbf{u}_{n+1} = \mathbf{u}_n + \Delta t\,\dot{\mathbf{u}}_n + (\frac{1}{2}-\beta)\,(\Delta t)^2\,\ddot{\mathbf{u}}_n \tag{42}$$

As the internal forces are calculated based on the values of the fields, the correction steps repeat the global procedure

$$\mathbf{M}_*\boldsymbol{\delta a} = \mathbf{F}_{ext} - \mathbf{F}_{int} \tag{43}$$

$$\mathbf{a}_{n+1} = \mathbf{a}_n + \boldsymbol{\delta a} \tag{44}$$

$$\dot{\mathbf{u}}_{n+1} = \dot{\mathbf{u}}_n + \alpha\,\Delta t\,\ddot{\mathbf{u}}_{n+1} \tag{45}$$

$$\mathbf{u}_{n+1} = \mathbf{u}_n + (\beta)\,\frac{(\Delta t)^2}{2}\,\ddot{\mathbf{u}}_{n+1} \tag{46}$$

until the norm of the relative correction

$$\frac{\|\boldsymbol{\delta a}\|}{\|\mathbf{a}\|} \tag{47}$$

as well as the relative flux

$$\frac{\|\mathbf{flux}\|}{\|\mathbf{energy}\|} \tag{48}$$

falls within predefined tolerance values. Equation (42) was solved with a direct solver from the Harwell Subroutine Library (HSLwww).

4 MESH MOVEMENT ALGORITHM

4.1 Mesh velocity criterion

The direction and velocity for moving all the nodes in a mesh can be either *explicit* (provided directly by the user or programmer) or *implicit* (based on some indirect criterion). While the former is easier to implement, an implicit technique is more general and requires less from the person running the simulations. In the context of combining grid motion with rigid body dynamics, the apparent difficulties in finding a suitable criterion coupled with knowledge of the motion of the train has lead to the choice of a semi-implicit method. As the rail wheel displacement is connected to the finite element track structure through a special type of constraint equations, it is possible to use the location and coefficients of the wheel nodes to select the rate of motion for the mesh. The direction should be explicitly set by the user to simulate commonly occurring rail geometry changes such as curves, slopes and turnouts.

The displacements of the slave node (wheel) $\mathbf{U_s}$ ($[U_{s1}, U_{s2,} U_{s3}]^T$ in three dimensions) is connected to those of the nodes on the rail surface in the element where the virtual node on the rail head will end up as a consequence of the time step through an especially developed constraint equation (Lane et. al., 2004). The idea is that the increment in displacements for the wheel during the time increment in the lateral and vertical directions are tied to the increments in displacements for the rail top nodes. This enforces the conditions of no derailment and no penetration into the track. The coordinates for the contact points are especially marked and used as a basis to calculate the rate of motion for the finite element mesh. Assume that the rail vehicle is connected to the rail at M points (wheel nodes). By identifying the positions (original coordinates + displacements) of the slave nodes as $\mathbf{x_{jk}}$ ($[x_{11}, x_{21,} x_{31}]^T$, $[x_{12}, x_{22,} x_{32}]^T$ etc. up to $[x_{1M}, x_{2M,} x_{3M}]^T$), one may calculate a "center of mobile constraint equations" corresponding to a position located centrally between the wheel nodes through a normal averaging operation

$$\mathbf{cec} \equiv \frac{\sum_{k=1}^{M} \mathbf{x_k}}{M} \tag{49}$$

The calculation of these coordinates is illustrated in Figure 3

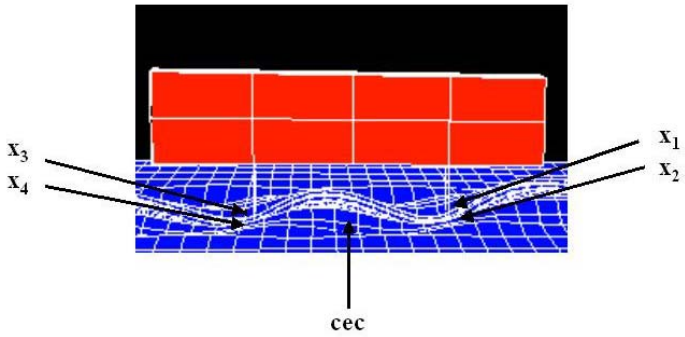

Figure 3: Centre of constraints.

The rate of mesh movement is then governed by the rate of change of this variable, i.e.

$$|\textit{Node coordinates (t) - Node coordinates (t-1)}| = |\,\mathbf{cec}(t) - \mathbf{cec}(t\text{-}1)| \tag{50}$$

The size of nodal movements is hence decided by the speed of the vehicle.

5 INTERPOLATING THE STATE

5.1 Finding Local Coordinates

As the nodes move to new locations, the values of displacements, velocities and accelerations should assume the values given by interpolations of the previous solution vectors for the nodes belonging to the element containing the new position. This is necessary to achieve a continuous and accurate solution. For this purpose, the solution process was preceded by creating a copy of the previous grid before motion, storing the positions of the nodes before moving them (see Figure 4).

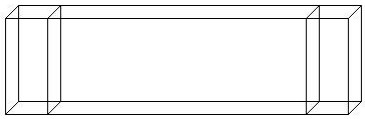

Figure 4: Previous grid copied before movement.

The old grid contains all the characteristics of the original mesh, including information about nodes, elements and field vectors. The sequence of operations is based on the strategy to find the values of displacements, velocities and accelerations at the positions where the nodes have been moved to. This builds on a standard FE shape function interpolation of the solution in the nodes. It is then necessary to find which element (in the previous grid) each node has been moved to and its local coordinates $\boldsymbol{\chi} = [\zeta, \xi, \eta]^T$ inside this element. The element number and local coordinates for an arbitrary point $\mathbf{x_p}$ is found through the following algorithm (Kettil and Wiberg, 2002)

1. Find the ten nodes closest to $\mathbf{x_p}$.
2. For each of these nodes, go through each element it is part of.
3. Search for the local coordinates of $\mathbf{x_p}$ in each element through a Newton-Raphson search. First, $\boldsymbol{\chi}$ is initialised to an arbitrary value $\boldsymbol{\chi_0}$. The following steps are then repeated until

$$|\mathbf{e_i}| \leq tolerance \tag{51}$$

   a. Find the 1x8 vector containing the values of the form functions $\mathbf{N}(\boldsymbol{\chi_i})$ and the 3x8 derivative matrix $\mathbf{B}=\tilde{\nabla}\,\mathbf{N}(\boldsymbol{\chi_i})$ evaluated at the point with the local coordinates $\boldsymbol{\chi_i}$.
   b. Find the corresponding search position $\mathbf{x_i}$ through the formula

$$\mathbf{x_i} = \mathbf{x_n}(\mathbf{N}(\boldsymbol{\chi_i})^{\mathbf{T}}) \tag{52}$$

   , where $\mathbf{x_n}$ is a 3x8 matrix containing the nodal locations (original coordinates + displacements) for the members of the solid brick element.
   c. Calculate the error

$$\mathbf{e_i} = \mathbf{x_i} - \mathbf{x_p} \tag{53}$$

   d. Check whether (49) is fulfilled. If the condition is met, $\mathbf{x_l} = \mathbf{x_i}$ and the iterations may stop. Otherwise, the search will continue.
   e. Find the matrix

$$\mathbf{D_i} = \mathbf{x_n}(\mathbf{B}(\boldsymbol{\chi_i})^{\mathbf{T}}) \tag{54}$$

   f. Solve the system of equations

$$\mathbf{D^i}\Delta\boldsymbol{\chi}^{\mathbf{i}} = -\mathbf{e^i} \tag{55}$$

   g. Update the local coordinate vector $\mathbf{x_i}$ as

$$\boldsymbol{\chi}^{\mathbf{i+1}} = \boldsymbol{\chi}^{\mathbf{i}} + \Delta\boldsymbol{\chi}^{\mathbf{i}} \tag{56}$$

If convergence according to (49) can't be reached within a predefined number of iterations or either of the local coordinates fall outside of the element ($\in$ j,[$|\chi_{ij}|$>1+*tol*χ], where *tol*χ is a

second user-defined tolerance) the search will continue for other elements connected to the node. If suitable local coordinates can't be found for any of these elements, it is concluded that the node has moved to a position completely outside the old mesh. In this case, displacements, velocities and accelerations will retain their values from the preceding time increment.

In order to achieve a correct time evolution of all node (displacements, velocities and accelerations) and element (stresses, strains, state variables and energy) field variables throughout the simulation, the values of these field variables should change when the mesh is subject to motion as determined by the previous state in the nodes surrounding the new positions (see Figure 5).

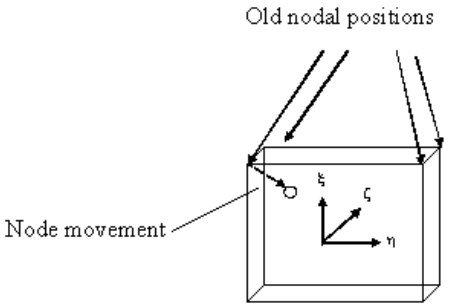

Figure 5. Interpolation of states.

A pre-requisite for this interpolation is knowledge about what element each node has moved into and the local coordinates of the new position. This information can be obtained with the search algorithm presented above, where the data was used to determine what direction every individual node should take. There is one important difference. Whereas the search with the purpose of deciding which nodes should be moved according to the user's specification was performed in the *initial* grid, the search with the aim of setting up interpolation is done in the *previous* mesh. While the copy of the original mesh is retained throughout the simulations, this object has to be created, copied and later destroyed in every time increment.

For nodes moving to coordinates *inside* the previous mesh, the search algorithm yields an element number other than 0. Assume that the local coordinate vector inside the element is denoted $\boldsymbol{\chi}$. The element's 3 x 8 matrix consisting of a collocation of the individual displacements from the former time step is called $\mathbf{u}_e$. The new field vectors for the node under consideration will then be given by

$$\mathbf{u}_m = \mathbf{u}_e \mathbf{N}(\boldsymbol{\chi})^T \tag{57}$$

$$\dot{\mathbf{u}}_m = \dot{\mathbf{u}}_e \mathbf{N}(\boldsymbol{\chi})^T \tag{58}$$

$$\ddot{\mathbf{u}}_m = \ddot{\mathbf{u}}_e \mathbf{N}(\boldsymbol{\chi})^T \tag{59}$$

$$\boldsymbol{\sigma}_m = \boldsymbol{\sigma}_e \, \mathbf{N}(\chi)^T \tag{60}$$

$$\boldsymbol{\varepsilon}_m = \boldsymbol{\varepsilon}_e \, \mathbf{N}(\chi)^T \tag{61}$$

The 1 x 8 **N** matrix contains the value of the form functions for the nodes in the new element.

6 ANALYSIS OF WAVE PROPAGATION OVER LONG DISTANCES

6.1 Setup

6.1.1 Overview

The aim of the simulations is to use the basic computational model defined in Chapter to predict the waves emanating from the wheel-rail interface of an X2 locomotive running over a rail structure. In order to evaluate the required size of the mesh, only a portion of the grid used in previous simulations (Lane et al., 2004), (Lane et al., 2006), (Lane et al., 2005) was used. The parameter *d* as shown in Figure 6 represents the distance from the front and wheel sets to the respective ends in the direction of travel.

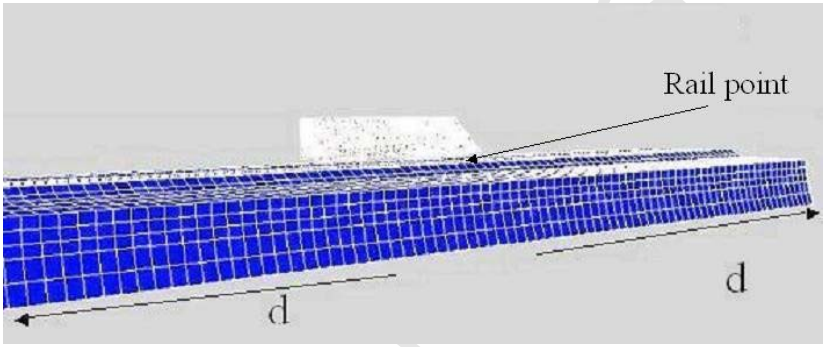

Figure 6. Size of model.

The boundary conditions were the same as those defined in a study on the same problem with moving loads (Ekevid et al., 2006) augmented with the usage of viscoelastic fictitious elements to absorb reflections (Lane et al., 2006). This means that the clay part of front and end of the mesh (Figure 7) is locked in all directions, while all degrees of freedom at the termination of the appended viscoelastic elements to the side and at the bottom are locked.

6.1.2 Dimensions

The locomotive consists of the car body and two bogies with two wheel axes each with overall dimensions according to Figure 7. The car, the bogies and the wheels are modeled by rigid elements. Springs and dampers model the connections between the car and the bogies and between the bogies and the wheels. Table 1 gives the mass and Table 2 shows the stiffness and damping properties.

The track consists of sleepers and rail, and the ground consists layers of ballast, dry crust and clay resting on rock with dimensions as given by Figure 7, and with material properties according to Table 3. The track and ground are modeled by elastic 8-node brick elements with a typical dimension of 0.7 m. Table 4 shows the properties of the absorbing layers.

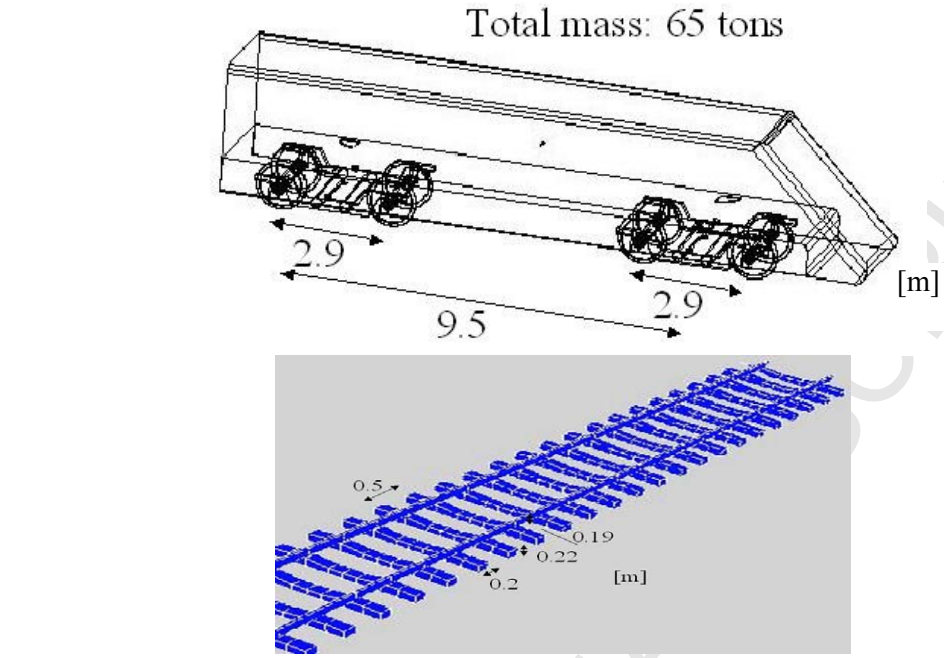

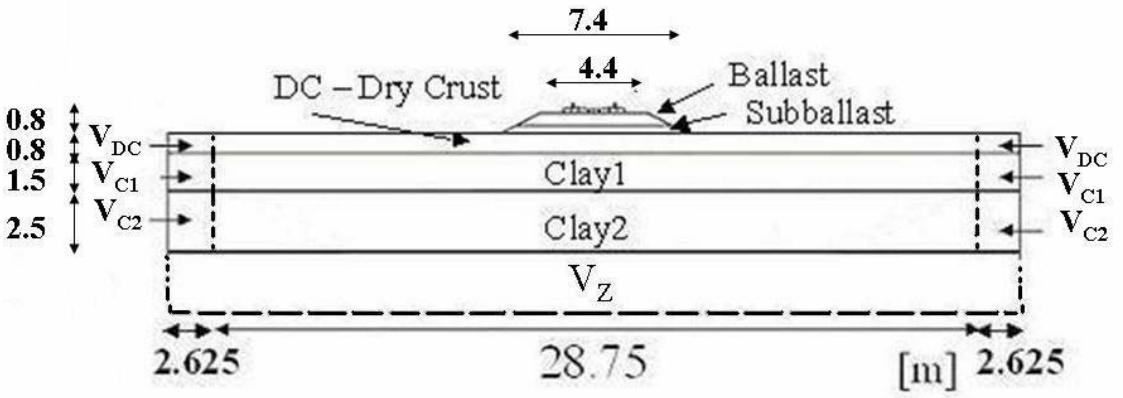

Figure 7: Model of X2000 train, track and ground.

	Weight / kg
Car body	54000
Boogies	2x3000
Wheels	8x1800

Table 1. Locomotive mass properties.

	K_v / (N/m)	K_h / (N/m)	D_v / (Ns/m)	D_h / (Ns/m)
Car to bogie	$1000x10^3$	$600x10^3$	$40x10^3$	$40x10^3$
Bogie to wheel	$1200x10^3$	$20x10^6$	$30x10^3$	$2x10^3$
Wheel to rail	$1200x10^4$	$20x10^7$	$30x10^4$	$2x10^4$

Table 2. Locomotive springs (K) and dampers (D) properties.

	ρ / (kg/ m³)	E / Pa	ν	η / (Pas)	c_R / (m/s)*
Rail	7820	206.8E9	0.29	0	-
Sleepers	2500	30E9	0.2	0	-
Ballast 1	1800	100E6	0.45	0	130
Ballast 2	1800	100E6	0.45	0	130
Dry crust	2000	30E6	0.45	0	67
Clay 1	2000	8E6	0.45	0	30
Clay 2	2000	13E6	0.45	0	40

Table 3. Track and ground material properties

*Rayleigh wave velocity.

The regions V_{DC}, V_{C1}, V_{C2} and V_z are fictitious elements with viscoelastic materials, which have been appended in order to absorb the outgoing waves and reduce reflections (Lane et. al. 2006). The material parameters in the crosssection are defined in Table 4. In the front and behind the elastic zone, each of the material layers defined in Figure 7 is joined to its respective viscoelastic domain of a length 0.3 m. The properties are based on formulae derived by Krenk et. al. (Krenk and Kierkegaard, 2001) and depends on the distance from the source (the wheel-rail interface) as well as the properties of the elastic region. The viscoelastic material parameters in the front and back are provided in Tabe 5 for the chosen *d* value of 16 m.

Absorbing layers	ρ / (kg/m³)	E / Pa	ν	η / (Pas)
V_{DC}	1	5.4783E6	0.45	3.3015E5
V_{C1}	1	1.4609E6	0.45	1.7049E5
V_{C2}	1	2.3739E6	0.45	2.1733E5
V_z	1	5.6670E6	0.45	2.0698E5

Table 4. Properties of absorbing layers in the *y* and *z* coordinate directions.

Absorbing layers	ρ / (kg/m³)	E / Pa in front	E / Pa behind	ν	η / (Pas)
V_x - Dry Crust	1	6.3291E5	6.016E5	0.45	3.7731E4
V_x – Clay1	1	1.6878E5	1.6043E5	0.45	1.9484E4
V_x – Clay2	1	2.7426E5	2.6070E5	0.45	2.4838E4

Table 5. Properties of absorbing layers in the *y* and *z* coordinate directions.

6.1.3 Time stepping parameters

A static step calculating the displacements from equilibrium between the applied forces of

gravity (Table 1) and internal stress forces was followed by a dynamic step. The rigid bodies were given a uniform velocity of 70 m/s (252 km/h) in the horisontal direction. This corresponds to a speed slightly above the wave propagation speed for the top layers in the ground (see Table 3). The consequence of this is that the ground will be in a critical state with strong vibrations spreading in certain directions. All nodes in the mesh were moved with the same speed. A time step of Δt = 0.03 s was used for the Newmark time integration. Average acceleration parameters (α = 0.5, β = 0.25) were assigned. The simulations ran on a single CPU on a Linux Redhat cluster.

6.2 Domain size analysis

One important choice concerns the assignment of a suitable value of the d parameter indicating the size of the mesh (see Figure 6). In order to make take full advantage of the opportunities of the moving mesh technique, an optimal value should not be higher than what is needed for accurate modelling of the vibrations in the soil. A series of tests were performed to find an appropriate distance.

6.2.1 Propagation

Figure 8a – c show the wave pattern (displaced mesh) with d = 10, 16 and 22 m respectively.

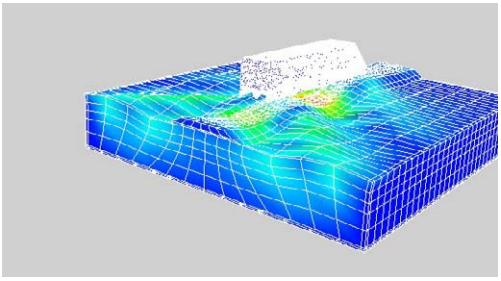

Figure 8a. Wave propagation with d = 10 m.

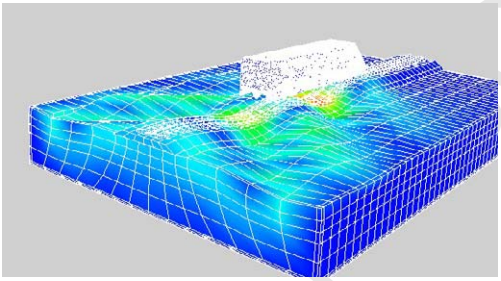

Figure 8b. Wave propagation with d = 16 m.

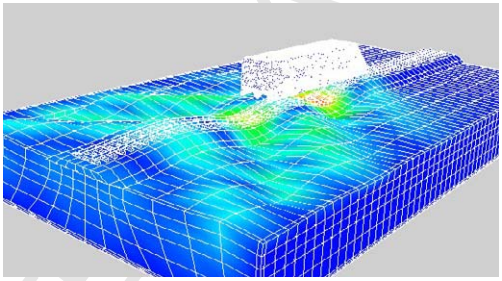

Figure 8c. Wave propagation with d = 22 m.

Although the displacements are magnified, the supersonic wave pattern for a velocity close to a critical speed for the structure is clearly revealed. The waves go out in the typical Mach cone directions with high amplitudes. The selection of a suitable distance for the mesh must be carried out with a balance between the desire to have enough elements for accurate results but not more than necessary. The inclusion of redundant parts will lead to too high computational demands without adding quality to the solution. The size of 10 m seems to cut the mesh in the middle of a wavefront and disregard a big part of the vibrations in the trail of the vehicle. The 22 m results seem to contain a portion with relatively low influence on the global behaviour. The distance of 16 m can be viewed as a reasonable size.

6.2.2 Displacement in point

A *fixed* point located just ahead of the front wheel set at the beginning of the analysis was chosen for analysis. As indicated in Figure 6, the point is located on the head of the rail at the right side 13.5 m ahead of the front wheel set when the train starts. The displacements for the

different *d* values are presented in Figure 9.

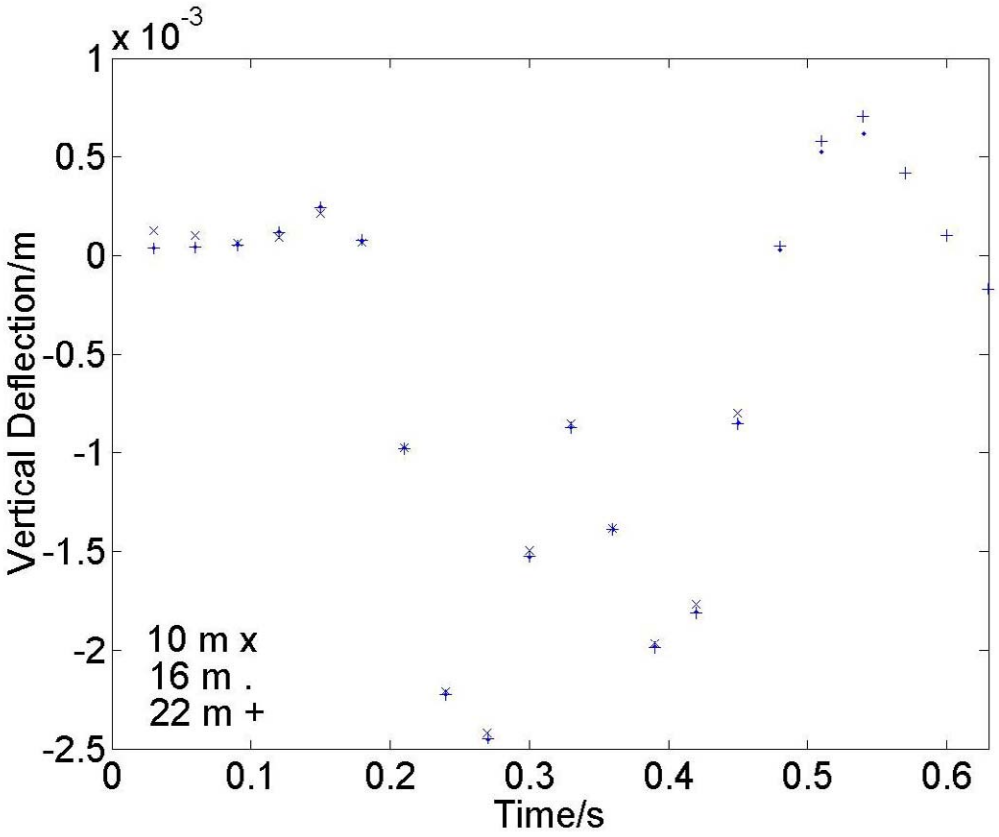

Figure 9. Displacements in point for different *d* values.

Note that values are missing for the shorter meshes, as the point under consideration is no longer in the analysed zone. The values for d = 16 and 22 m are nearly identical. The displacements for the distance of 10 m are somewhat different.

6.2.3 Efficiency

Table 5 presents the number of equations and time consumption per time increment (Δt) for the respective values of the parameter *d*. Calculations ran on a single node with a CPU of 2 Ghz on a Linux RedHat cluster.

d	Neq	Time per increment
10	26164	~ 150 – 180 s
16	36364	~ 180 – 200 s
22	45949	~ 210 - 220 s

Table 5. Computations for different mesh sizes.

The value of 16 m seems to offer a good tradeoff between accuracy and efficiency. It can be noted that computational times for a fixed mesh with a size of 89 m are in the order of 14 min, i.e. 5 - 6 times higher than those for the chosen grid. The size of 16 m was used for the rest of the presented simulations.

6.3 Fixed mesh comparisons

Figure 10 presents the displacements of the monitored rail point (Figure 6) for the moving mesh as compared to corresponding simulations with a large fixed mesh. The picture clearly demonstrates the similarity of the methods. The deviations towards the end can be explained by the fact that the train in the fixed mesh is very near the front boundary.

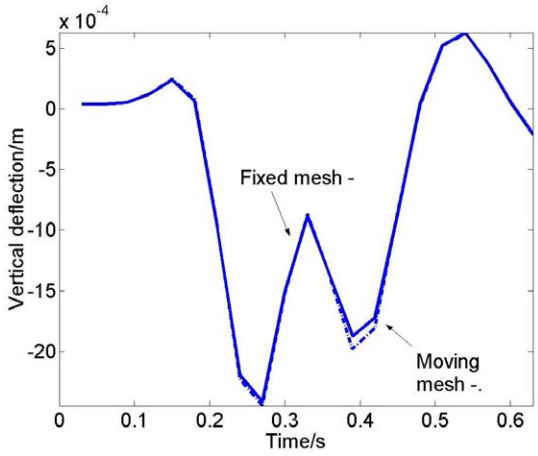

Figure 10. Results for fixed mesh and moving grid.

6.4 Wave propagation pattern

Figure 11a-c display the nature of the waves at three different time instants, with the train having traveled 57 m, 328 m and 636 m, respectively.

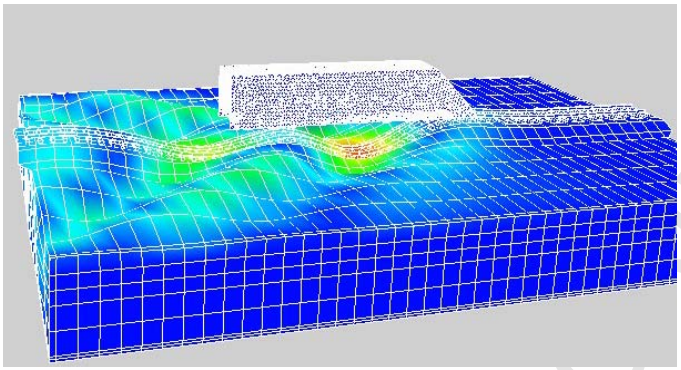

Figure 11a. Wave propagation alter a distance of 57 m.

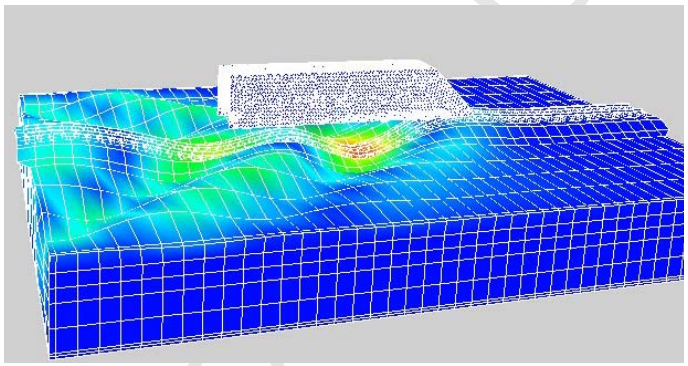

Figure 11b. Wave propagation after a distance of 328 m.

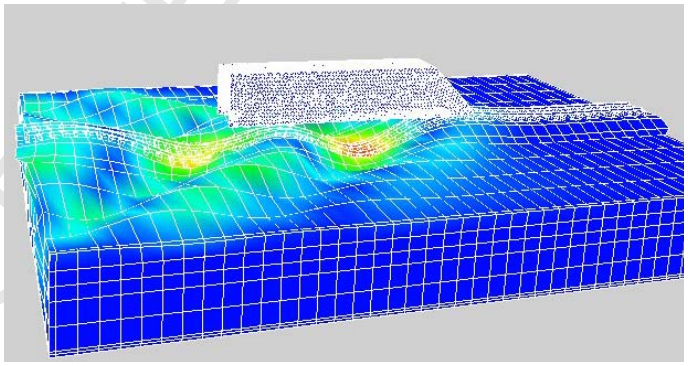

Figure 11c. Wave propagation after a distance of 636 m.

As expected, the wave patterns underneath the train are similar for the analysed sampling instants.

6.5 Critical speed effect

Figure 12a-c portrays the nature of the vibrations for a velocity below (50 m/s), just above (70 m/s) and far above (90 m/s) the velocity of Rayleigh waves in the top layer of soil.

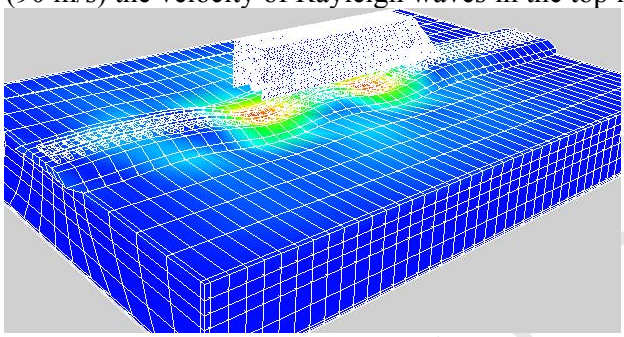

Figure 12a. Wave propagation for v = 50 m/s (180 km/h).

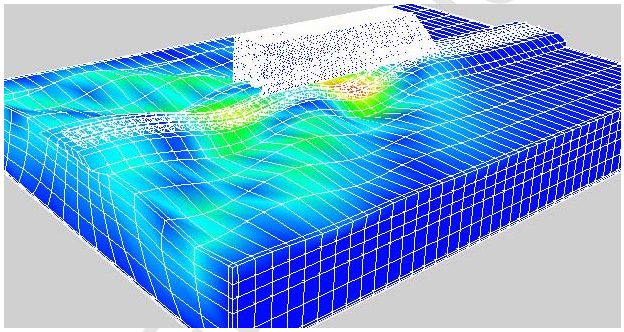

Figure 12b. Wave propagation for v = 70 m/s (252 km/h).

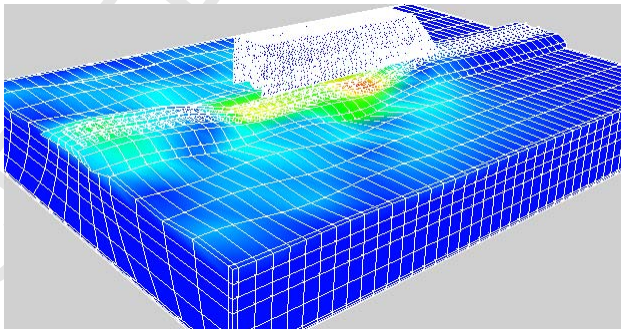

Figure 12c. Wave propagation for v = 90 m/s (324 km/h).

The critical speed effect identified in several other studies (Lane et al., 2004), (Larsson and Berg, 2005), (Ching 2004), (Ogwemoh 2005) and predicted by analytical studies (de Hoop 2002) is clearly demonstrated.

7 CONCLUSIONS

A moving mesh technique has been presented for finite element computations of elastic wave propagation. The method is based on concentrating the grid to a smaller part centered around the vehicle providing the excitation and moving the elements with the same speed as the source. Fields are interpolated based on finding the local coordinates and the corresponding value of the form functions for the element that the respective nodes move into.

It was found that a value of 15 m in front of the front wheel set and a similar distance behind the back wheels led to a good compromise between accuracy and efficiency. The results for this mesh were nearly identical with corresponding simulations with a large fixed mesh at 5-6 times lower computation times. The moving mesh approach has this served to make computations far more efficient.

The critical speed effect was clearly identified. Although the presented simulations were restricted to a straight structure with constant material parameters, the method can also be extended by changing material conditions or imposing an irregularity on the track. It can also be used in several other contexts.

8 ACKNOWLEDGMENTS

Financial support from the Swedish Railroad Administration (Banverket (Banverketwww)) and the Swedish Research Council for Environment, Agricultural Sciences and Spatial Planning (Formas (Formaswww)) is essential for the activities undertaken within the project and gratefully acknowledged. The administrative support and exchange of knowledge arranged by the Chalmers Railway Mechanics competence centre (Charmecwww) is also important. Usage of the free G95 compiler (G95www) has been very helpful during the programming stage.

The packages HSL (HSLwww), BLAS (BLASwww), LAPACK (LaPackwww), SuperLU (SuperLUwww) and METIS (METISwww) are included in the software.

A special thank you goes to the staff at the Department of Mathematics at the University of Reading. A major part of the development of the code for the method was done by Mr. Lane during a visit in the summer of 2005. They have freely and generously allotted their time and resources.

9 REFERENCES

Baines, M. J., 2002. Moving meshes, conservation laws and least squares equidistribution, International Journal on Numerical Methods in Engineering 40, 3-20.

Budd, C. J., Collins, G. J., 1998. An invariant moving mesh scheme for the nonlinear diffusion equation, Applied Numerical Mathematics 26, 23-39.

Ching, C. Y. R., Finite Element Rail Vibration Dynamics: Multi-body Dynamics of Modern High-speed Trains, 2004. Master Thesis 04:15, Department of Structural Engineering and Mechanics, Chalmers University of Technology, Gothenburg, Sweden.

de Hoop A., 2002. The moving-load problem in soil dynamics – the vertical approximation, Wave Motion 36, 335-346.

Ekevid, T., Lane, H., Wiberg, N-E., 2006. Adaptive solid wave propagation—influences of boundary conditions in high-speed train applications, Computer Methods in Applied Mechanics and Engineering 195, 236-250.
Forster, H., Schrefl, T., Suess, D., Scholz, W., Tsiantos, V., Dittrich, R., Fidler, J., 2002. Domain wall motion in nanowires using moving grids. Journal of Applied Physics 91, 6914-6919.
Gwynllyw, R., Davies, A. R., Phillips, T., 1996. A moving spectral element approach to the dynamically loaded journal bearing problem, Journal of Computational Physics 2, 476-494.
Kettil, P., Wiberg, N.-E., 2002. Application of 3D Solid Modeling and Simulation Programs to a Bridge Structure, Engineering with Computers 18, 160-169.
Krenk, S., Kierkegaard, P. H., 2001. Local tensor radiation conditions for elastic waves, Journal of Sound and Vibration 247, 875-896.
Lane, H., Berg, S., Larsson, M., 2005. Finite Element Calculations of Rail Vibration Countermeasures, Submitted to Vehicle System Dynamics.
Lane, H., Ekevid, T., Wiberg, N.-E., Vehicle-Track-Underground Modelling of Train Induced Wave Propagation, 2004. Presented at the ECCOMAS conference in Jyväskylä in July 2004 and Submitted to Computers and Structures.
Lane, H., Kettil, P., Enelund, M., Ekevid, T., Wiberg, N.-E., 2006. Absorbing Boundary Layers for Elastic Wave Propagation. Submitted to Applied Mathematical Modelling.
Larsson, M., Berg, S., Finite Element Rail Vibration Dynamics – Ground Improvement with Lime-Cement Column, 2005. Diploma Work 2005:12, Department of Applied Mechanics, Chalmers University of Technology, Gothenburg, Sweden.
MacNeal, R., 1994. Finite Elements: their design and performance, M. Dekker, New York, United States of America.
Ogwemoh, G. G., 2005. Finite Element Rail Vibration Dynamics – Influence of Track Irregularities, Diploma Work 2005:79, Department of Applied Mechanics, Chalmers University of Technology, Gothenburg, Sweden.
Samuelsson, A., Wiberg, N.-E., 1998. Finite Element Method – Basics, Studentlitteratur, Lund, Sweden.
Stahel, A., 1999. Calculus of Variations and Finite Elements, Hochshule für Technik und Informatik, Berner Fachhochshule, Switzerland.
Wittenburg, J., 1977. Dynamics of Systems of Rigid Bodies, B. G. Teubner, Stuttgart, Germany.

Web references:
http://crd.lbl.gov/~xiaoye/SuperLU/index.html - SuperLU. Latest access 29/3-2004.
http://www.banverket.se – Banverket. Latest access 2/5-2006.
http://www.charmec.chalmers.se – Charmec. Latest access 2/5-2006.
http://www.cs.colorado.edu/~lapack/ - LAPACK. Latest access 29/3-2004.
http://www.formas.se –Formas. Latest access 2/5-2006.
http://www.g95.org – G95. Latest access 2/5-2006.
http://www.netlib.org/blas/ - BLAS. Latest access 29/3-2004.
http://www-users.cs.umn.edu/~karypis/metis/ - METIS: Family of Multilevel Partitioning Algorithms.

Latest access 16/4-2004.